Biological effects in unirradiated human tissue induced by radiation damage up to 1 mm away

Oleg V. Belyakov*†, Stephen A. Mitchell*, Deep Parikh‡, Gerhard Randers-Pehrson*, Stephen A. Marino*, Sally A. Amundson*, Charles R. Geard*, and David J. Brenner*§

*Center for Radiological Research, Columbia University, New York, NY 10032; †Radiation Biology Laboratory, Research and Environmental Surveillance, Radiation and Nuclear Safety Authority, P.O. Box 14, FIN-00881, Helsinki, Finland; and ‡Stuyvesant High School, New York, NY 10282

Edited by Richard B. Setlow, Brookhaven National Laboratory, Upton, NY, and approved August 3, 2005 (received for review June 16, 2005)

A central tenet in understanding the biological effects of ionizing radiation has been that the initially affected cells were directly damaged by the radiation. By contrast, evidence has emerged concerning "bystander" responses involving damage to nearby cells that were not themselves directly traversed by the radiation. These long-range effects are of interest both mechanistically and for assessing risks from low-dose exposures, where only a small proportion of cells are directly hit. Bystander effects have been observed largely by using single-cell *in vitro* systems that do not have realistic multicellular morphology; no studies have as yet been reported in three-dimensional, normal human tissue. Given that the bystander phenomenon must involve cell-to-cell interactions, the relevance of such single-cell *in vitro* studies is questionable, and thus the significance of bystander responses for human health has remained unclear. Here, we describe bystander responses in a three-dimensional, normal human-tissue system. Endpoints were induction of micronucleated and apoptotic cells. A charged-particle microbeam was used, allowing irradiation of cells in defined locations in the tissue yet guaranteeing that no cells located more than a few micrometers away receive any radiation exposure. Unirradiated cells up to 1 mm distant from irradiated cells showed a significant enhancement in effect over background, with an average increase in effect of 1.7-fold for micronuclei and 2.8-fold for apoptosis. The surprisingly long range of bystander signals in human tissue suggests that bystander responses may be important in extrapolating radiation risk estimates from epidemiologically accessible doses down to very low doses where nonhit bystander cells will predominate.

bystander | normal human tissue | radiological risk

A central tenet in our understanding of radiation-induced biological damage has been that the initially affected cells were directly damaged by the radiation, either by the radiation track itself or through consequent nanometer-ranged, short-lived free radicals. By contrast, a range of evidence has now emerged concerning so-called "bystander" responses involving damage to cells that were not directly traversed by ionizing radiation, being located at significant distances from the directly hit cells. Bystander effects were first reported for the endpoint of sister chromatid exchanges (1); since then, they have been observed for many endpoints, including clonogenic survival, chromosome aberrations, apoptosis, micronuclei, *in vitro* oncogenic transformation, mutation induction, genomic instability, and changes in gene expression (2–8). *In vitro*, bystander effects have been observed to be mediated by direct gap-junction signaling (9) as well as by molecules secreted into medium (10). Such long-range effects are of interest both mechanistically (11) and for assessing the risk from a low-dose exposure to a carcinogen such as ionizing radiation, where only a small proportion of cells are actually directly hit (12).

Almost all bystander-effect studies to date have been carried out by using conventional single-cell *in vitro* systems that do not have a realistic three-dimensional, multicellular structure (2–8). A few studies have been reported in monolayer explants (13–15), but no studies have as yet been reported in normal, three-dimensional human tissue. Given that the bystander phenomenon must involve cell-to-cell communication, directly or indirectly, the relevance of single-cell studies is questionable; thus, experimental models that maintain tissue-like intercellular signaling and three-dimensional structure are important to assess the relevance of bystander responses for human health (16) (in particular, to estimate the range of these bystander signals in human tissue). Here, we report bystander responses in a three-dimensional, normal human tissue system; specifically, a reconstructed human skin model is used. This study is made possible by the use of a charged-particle microbeam (17), which allows irradiation of cells in defined locations in the tissue yet guarantees that cells more than a few micrometers away receive no radiation exposure.

Bystander responses have been reported in single-cell systems for endpoints that might be considered detrimental [such as mutational or chromosomal damage (2–4, 6, 7)] as well as protective against carcinogenesis [such as cell killing (18, 19)]. Consequently, in this study, we have chosen one endpoint from each category: induction of micronuclei and induction of apoptotic cell death.

Methods

Reconstructed Human Skin Systems. We report bystander responses in two types of reconstructed, normal human three-dimensional skin tissue systems (MatTek, Ashland, MA), shown in Fig. 1. These systems are generated by growing differentiated keratinocyte cultures on acellular or fibroblast-populated dermal substrates (20, 21). One of the systems reconstructs the human epidermis, and the other is a "full-thickness" skin model corresponding to the epidermis and dermis of normal human skin.

Morphologically, these reconstructed tissues show very similar microarchitectures to the corresponding tissue *in vivo*: Epidermal layers of the skin models consist of basal, spinous, granular, and cornified layers, analogous to those found *in vivo*. Analysis of the tissue microstructure has demonstrated the presence of keratohyalin granules, tonofilament bundles, desmosomes, and a multilayered stratum corneum containing intercellular lamellar lipid layers arranged in patterns characteristic of the *in vivo* epidermis (22). The reconstructed tissues are mitotically and metabolically active, maintaining the same differentiation patterns as those *in vivo* (21, 23). Markers of mature epidermis-specific differentiation such as profilaggrin, the K1/K10 cytokeratin pair, involucrin, and type I epidermal transglutaminase, are expressed (24). The reconstructed tis-

This paper was submitted directly (Track II) to the PNAS office.

Freely available online through the PNAS open access option.

See Commentary on page 14127.

§To whom correspondence should be addressed at: Center for Radiological Research, Columbia University, 630 West 168th Street, New York, NY 10032. E-mail: djb3@columbia.edu.

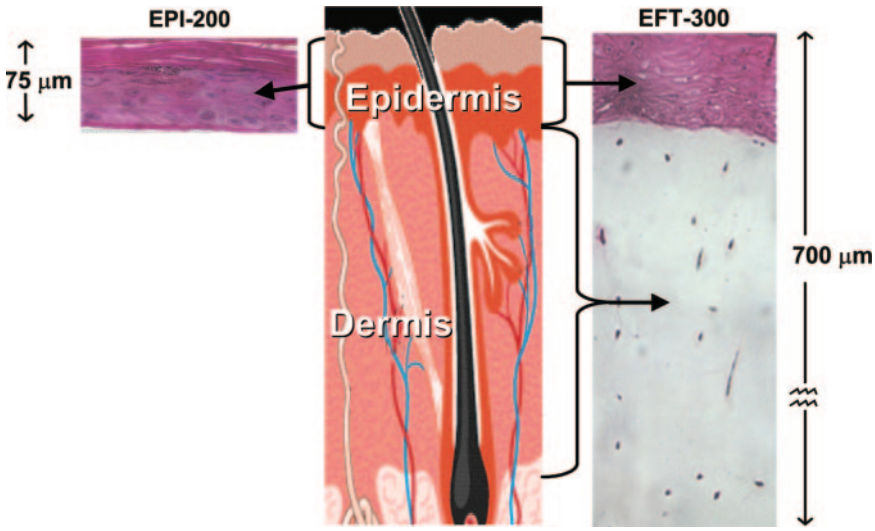

Fig. 1. The two reconstructed normal human skin tissue systems used here. Shown are the keratinocyte-containing epidermis (EPI-200, *Left*) and full-thickness skin (EFT-300, *Right*), consisting of a dermal layer containing fibroblasts and an epidermal layer similar to that in EPI-200, containing keratinocytes.

sues show lipid profiles similar to the corresponding tissue *in vivo*, release the relevant cytokines, and demonstrate the presence of gap junctions (21–24).

These reconstructed tissues are very stable and allow a high degree of experimental reproducibility (25).

Reconstructed Epidermis. The model of the human epidermis (Fig. 1 *Left*, designated EPI-200) consists of normal human epidermal keratinocytes that have been cultured to form a multilayered, differentiated model of the human epidermis (20). It closely resembles human epidermal microarchitecture (see above), with *in vivo*-like morphological and growth characteristics that are uniform and highly reproducible. It contains 8–12 cell layers and is ≈75-μm thick.

Reconstructed Full-Thickness Skin. The model for full-thickness skin (Fig. 1 *Right*, designated EFT-300) contains both an epidermal layer containing keratinocytes and a dermal layer containing fibroblasts and extracellular matrix. These layers correspond to the epidermis and dermis of normal human skin and are cultured from normal human epidermal keratinocytes and dermal fibroblasts. Histological cross sections of this full-thickness tissue demonstrate an ''epidermal'' layer that is very similar to the EPI-200 model (see above) on top of a fibroblast-containing, collagen matrix dermis-like layer. The overall thickness of this tissue is ≈700 μm.

Tissue Culture. The reconstructed tissues were cultivated by using an air–liquid interface tissue culture technique: The tissue is grown on a semipermeable membrane, fed with serum-free medium from below, and cultivated on Millicell-CM culture inserts (Millipore) by using a 28-μm hydrophilic membrane. The surface of the tissue is exposed to the air, which stimulates differentiation. The diameter of the tissues is 8 mm, and their useful lifetime is 2–3 weeks.

Microbeam Irradiation. To be able to produce direct radiation damage in cells spatially defined locations in the three-dimensional tissue, and guarantee no direct radiation damage to the remainder of the cells in the tissue, the Columbia University charged-particle microbeam was used. The charged-particle microbeam delivers defined numbers of charged particles (in this case, α-particles) with high accuracy to specified locations. The charged particles are focused with a series of electrostatic lenses (26) to a beam diameter of <5 μm. A detailed description of the microbeam is given in ref. 17. In the current experiments, 7.2-MeV α-particles were used (range $\sim$ 60 μm; initial stopping power of 80 keV/μm). As schematized in Fig. 2, each tissue sample was irradiated with the microbeam such that all of the irradiated cells were in a single thin vertical plane, of thickness no more than two cell diameters, which bisects the tissue sample. Because the α-particles scatter very little ($\ll$1 μm) as they pass through the tissue sample, the arrangement guarantees that cells more than a few micrometers away from the plane of irradiated cells will receive a zero radiation dose.

Irradiation Protocols. The tissue samples were irradiated from below through the membrane that forms the base of the culture insert. The insert was positioned in a custom-designed holder attached to the microbeam stage, with a repositioning accuracy of better than 2 μm. Ten α-particles were delivered every 100 μm along a diameter of each tissue, corresponding to 80 locations across the tissue diameter. Typical total irradiation times were ≈2 min per tissue.

For the EPI-200 epidermal tissue, a given α-particle will traverse 5–10 cells as it penetrates the tissue; thus, as 80 locations across a diameter of tissue were microbeam-irradiated, a total of 400–800 cells located in the designated irradiation plane were actually traversed by α-particles, with each traversed cell receiving an average dose of ≈1 Gy.

For the full-thickness skin (EFT-300) experiments, separate protocols were used to irradiate the tissue from the dermal and the epidermal sides. Thus, one protocol directly targeted only keratinocytes in the epidermis, and the other directly targeted only fibroblast cells (and extracellular matrix) in the dermis. In each case, the keratinocyte cells in the epidermal layer were subsequently assayed for apoptotic cell frequency as a function of the distance from the irradiated plane. No assays were undertaken in dermal fibroblasts because of their low density.

Distance-Dependent Assays. After microbeam irradiation of a single plane across the tissue diameter, each tissue was returned to a multiwell dish filled with fresh medium and incubated at 37°C in a humidified atmosphere with 5% CO_2. At 72 h postirradiation, the tissues were formalin-fixed, paraffin-embedded, and sectioned into 5-μm-thick strips parallel to the

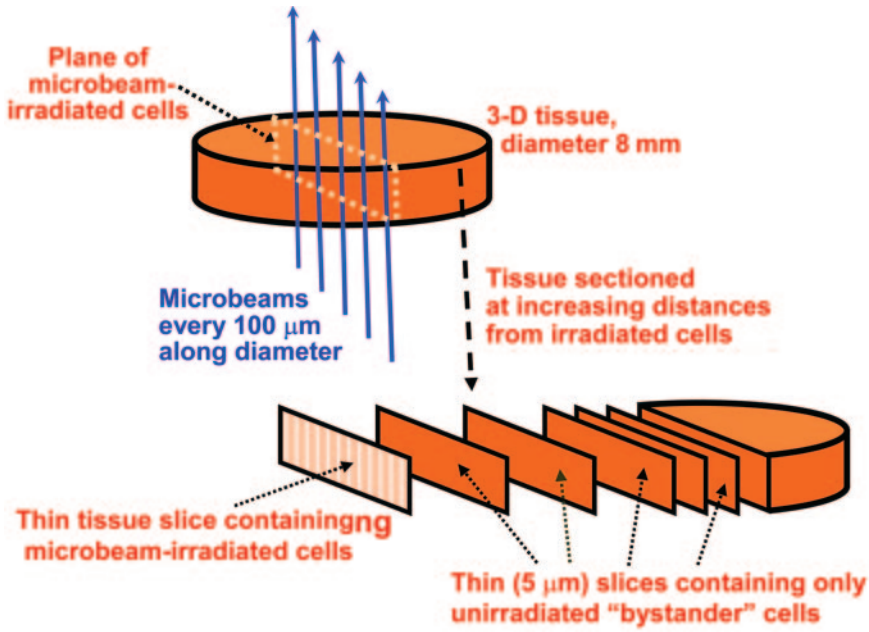

Fig. 2. Schematic of the irradiation procedure. Each tissue sample consists of an 8-mm-diameter cylinder that is 75 μm (epidermal model, EPI-200) or 700 μm (full-skin model, EFT-300) in height that is microbeam-irradiated along a diameter by α-particles (10 particles every 100 μm along the diameter). The microbeam is <5 μm across, less than one cell diameter, so the plane of irradiated cells is no more than two cells wide. After irradiation, the tissue is fixed and sectioned into 5-μm slices parallel to, and progressively farther from, the irradiated plane of cells.

plane of irradiated cells (see Fig. 2). As illustrated in Fig. 2, this protocol allows separate analysis of slices of tissue containing only nonirradiated cells, each slice having been located at increasing and known distances from the plane of irradiated cells.

An estimate of the shrinkage produced in the fixed, embedded samples was made by comparing morphometric data obtained with unfixed vs. fixed samples. Shrinkage of $\approx$10% in each direction was observed, as described in ref. 27.

Distance-Dependent Apoptosis Assay. Apoptotic cells were scored in each section on day 3 postirradiation by using a TUNEL (28) enzymatic *in situ* labeling kit (DermaTACS, Trevigen, Gaithersburg, MD) optimized for paraffin sections. This time was chosen based on preliminary experiments to reflect the maximal apoptotic response. Some typical images are shown in Fig. 3. The fractions of apoptotic cells were assessed in 5-μm-thick tissue slices at distances from 200 to 1,100 μm from the plane of irradiated cells and compared with corresponding controls for

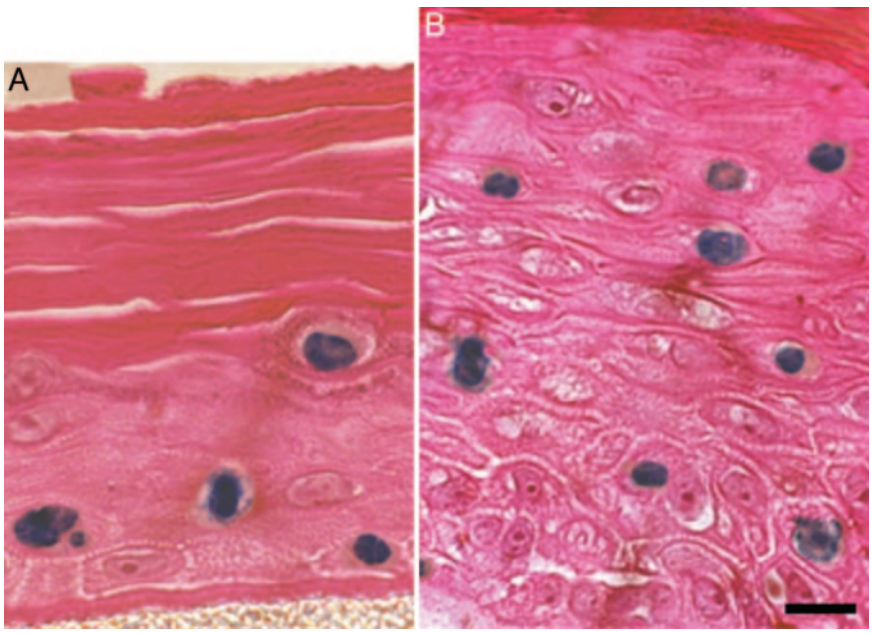

Fig. 3. Examples of apoptosis in unirradiated bystander cells in artificial human skin systems. Shown are EPI-200 (*A*) and EFT-300 (*B*) stained with a DermaTACS apoptosis kit; positive apoptotic cells appear blue. Each slice of tissue shown was $>$200 μm from the plane of irradiated cells and thus received no direct or scattered radiation exposure. Formalin-fixed, paraffin-embedded, 5-μm-thick histological sections are shown. (Scale bar: 10 μm.)

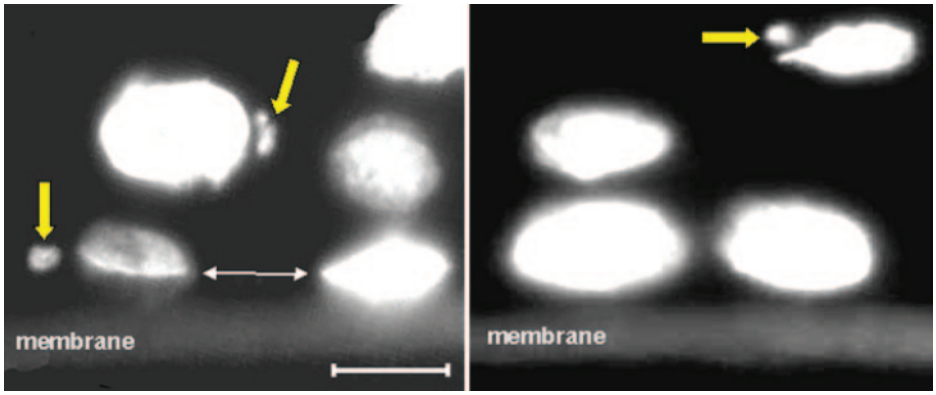

Fig. 4. Micronuclei observed in unirradiated bystander cells in three-dimensional epidermal tissue (EPI-200) stained with DAPI. Each slice of tissue shown was >200 μm from the irradiated cells and thus received no direct or scattered radiation exposure. The support membrane can be seen at the bottom of each image. The large arrows indicate micronuclei associated with individual cell nuclei. The small arrows show the location of a broken nucleoplasmic bridge, indicating, as expected, a plane of cellular division parallel to the membrane. (Scale bar: 10 μm.)

which the central plane of cells had been sham-irradiated. At each distance, a total of ≈10,000 cells were scored in three repeat samples.

Distance-Dependent Micronucleus Assay. Three days were allowed postirradiation for cell proliferation and division to continue. Tissues were then fixed in formalin and paraffin-embedded, and 5-μm sections were sliced at 100-μm intervals parallel to the plane of microbeam irradiation (different slices thus having been at increasing distances from the irradiated cells). The tissue sections on microscope slides were stained with DAPI, a fluorescent DNA-binding dye that labels all cell nuclei and micronuclei.

Micronuclei and/or nucleoplasmic bridges will result from aberrant mitotic divisions involving chromosomal aberrations. Such events, examples of which are shown in Fig. 4, are readily induced by ionizing radiation and have been seen, *in vitro*, in cells that were known bystanders of known irradiated cells (29). Frequencies of cell nuclei with associated micronuclei, relative to all nuclei, were recorded in three 500-cell samples at each plane at different distances (200–1,100 μm) from the plane of irradiated tissue, as well as the sham-irradiated control tissues.

Controls. The control tissues were handled in exactly the same manner as the irradiated samples, except that the central plane of cells (Fig. 2) was sham-irradiated (i.e., the microbeam was not turned on, so no cells were irradiated).

Statistical Analyses. For the control cells (those in the same location at which bystander responses were probed, but for sham-irradiated tissue samples), to see whether the location of the sample within the tissue was significant apart from any bystander effects, a standard Poisson homogeneity test (30) was performed, intercomparing the results from each slice.

For the nonirradiated cells in the irradiated tissue, we compared the results by using Fisher's exact test (31), both with the control sample from the same location and, when appropriate (see homogeneity test, above), with the pooled controls from all locations.

Results

For the epidermal skin tissue (EPI-200), Fig. 5 shows the measured fractions of apoptotic cells and micronucleated cells. All of the data shown are for unirradiated tissue, plotted as a function of distance from the irradiated cells or (for the controls) the sham-irradiated cells.

For the control cells (those in the same location at which bystander responses were probed, but from sham-irradiated tissue samples), the results for both endpoints were independent of the location within the tissue ($P > 0.25$ using an exact homogeneity test).

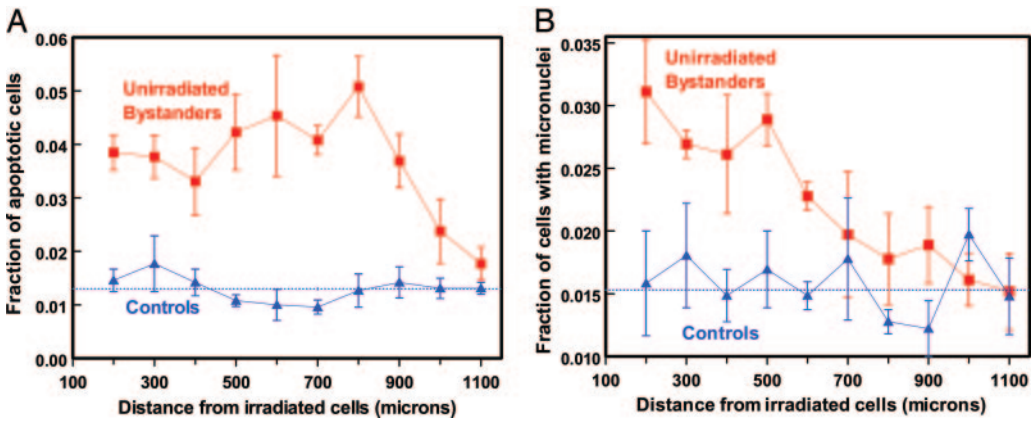

Fig. 5. Fraction of apoptotic (*A*) and micronucleated (*B*) cells in unirradiated bystander cells at different distances from the plane of irradiated cells in a three-dimensional human epidermal skin model (EPI-200). Controls refer to sham irradiations, with conditions otherwise identical. Dotted lines show mean value of control points. Each data point (and SEM) is derived from experiments with three independent tissues.

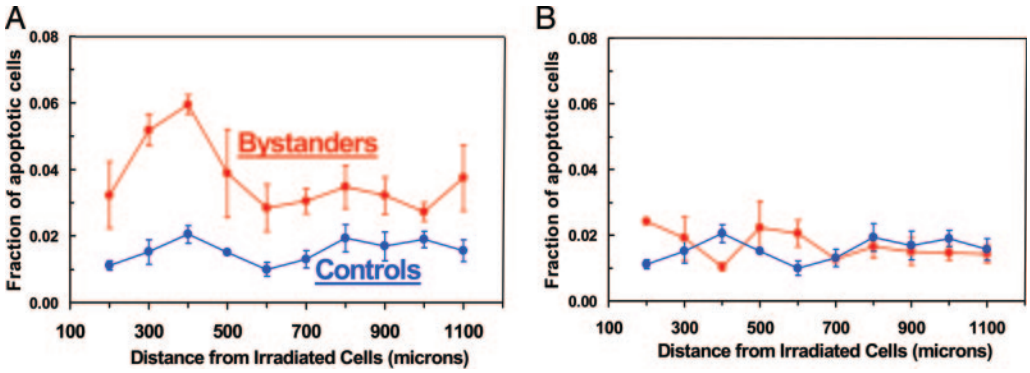

Fig. 6. Fraction of apoptotic cells in unirradiated keratinocyte layers at different distances from a plane of irradiated cells in a three-dimensional, full-thickness human skin model (EFT-300). Controls refer to sham irradiations, with conditions otherwise identical. Each data point (and SEM) is derived from studies with three independent tissues. (*A*) Microbeam irradiation of a plane of cells only in the epidermal layer, showing a significant bystander response. (*B*) Microbeam irradiation of a plane of cells only in the dermal layer, showing no evidence of a bystander response in the unirradiated epidermal layer.

For the apoptotic endpoint, a statistically significant bystander response in unirradiated cells relative to the controls was observed at all distances up to 1,000 μm (1 mm) away from the irradiated cells ($P < 0.05$ at each distance, Fisher's exact test, two-sided). Averaged over distances from 200 to 1,000 mm from the plane of the irradiated cells, the mean proportion of apoptotic cells was 3.7 $\pm$ 0.6% in the bystander cells vs. 1.3 $\pm$ 0.3% in the controls. The bystander-related enhancement in effect over controls was a factor of 2.6 $\pm$ 0.4 at a distance of 200 μm from the irradiated cells, and the corresponding enhancement, averaged over all distances from 200 to 1,000 μm, was a factor of 2.8 $\pm$ 0.3.

For micronucleus induction, a statistically significant bystander response, relative to the controls, is apparent in unirradiated cells at all distances up to 600 μm (0.6 mm) away from the irradiated cells ($P < 0.05$ at each distance, Fisher's exact test, two-sided). The bystander-related enhancement in effect relative to controls was a factor of 2.0 $\pm$ 0.4 at a distance of 200 μm from the irradiated cells, and the corresponding enhancement, averaged over all distances from 200 to 600 μm, was a factor of 1.7 $\pm$ 0.3.

Fig. 6 shows the results with the full-thickness skin model (EFT-300), which contains an epidermal keratinocyte layer on one side and a fibroblast-containing dermal layer on the other. Separate protocols were used to irradiate the full-thickness tissue from the epidermal side and the dermal side, each with α-particles of range $\sim$ 60 μm; thus, one protocol irradiates only a plane of epidermal keratinocytes, and the other irradiates only a plane of dermal fibroblasts (plus extracellular matrix) within the 700-μm-thick tissue. The fraction of apoptotic cells in the keratinocytes in the epidermal layer was assessed as above in unirradiated tissue sections that were at increasing distances from the plane of the irradiated cells.

When the epidermal layer in the full-thickness tissue was irradiated (Fig. 6*A*), there was a clear bystander response extending to 1,100 μm ($P < 0.05$ at each distance, Fisher's exact test, two-sided); this response was very similar to that when the epidermis-only system (EPI-200) was studied (Fig. 5*A*). However, when only the dermal region containing fibroblasts (and extracellular matrix) was irradiated, no bystander response was seen in the keratinocytes (Fig. 6*B*). This observation may suggest that there is no signaling from the dermal to the epidermal layers in terms of the bystander response, although it could simply be the consequence of the distance ($\geq$600 μm) between the irradiated dermal cells and the probed unirradiated keratinocytes.

Discussion

In summary, we have shown that unirradiated human cells in normal, three-dimensional human tissue systems can respond to radiation-induced cellular damage that occurs in cells at quite large distances away. Specifically, the results suggest that the bystander response is propagated over distances up to 1 mm in normal human tissue. We have demonstrated this effect both for a cytogenetic damage endpoint (at distances up to 0.6 mm), which might be expected to be associated with deleterious consequences, and a cell-killing endpoint (at distances up to 1 mm), which, through the elimination of damaged cells, could be associated with protective consequences. Bystander responses for both potentially protective and potentially deleterious endpoints have also been reported in *in vitro* single-cell experimental systems (2–4, 6, 7).

The magnitude of the bystander response was clearly statistically significant for both the apoptotic and the micronucleus endpoints, although the magnitude of the response is clearly less than for directly hit cells. For example, based on *in vitro* results (32), the frequency of micronucleated cells among those cells that were directly hit by α-particles (based on a dose of $\sim$1 Gy to these hit cells) would be $\approx$0.25, compared with a maximum frequency of micronucleated cells that we observed among unirradiated bystander cells of 0.03. In contrast, given a bystander-signal range of up to 1 mm, in most low-dose situations, there will be far more potential bystander cells than hit cells.

The shape of the curves in Fig. 3 (relatively flat over a distance of several hundred micrometers) suggests, as have much other data from single-cell systems (19, 33), that bystander effects are characterized by a binary threshold response (i.e., unirradiated cells respond in a binary way to a damage signal, as long as the intensity of the signal remains above a threshold value). The range of the bystander signal in tissue, up to 1 mm, corresponds to $\approx$50–75 cell diameters. This surprisingly long range implies either that directly damaged cells produce long-range, diffusible bystander signals, perhaps through autocrine/paracrine mechanisms (34–37), or that a cell relay system is active, in which cells signal only their immediate neighbors (juxtacrine signaling), the signal being relayed by spatially intermediate, unirradiated bystander cells (38–40).

In terms of potential consequences, bystander responses have been hypothesized to be significant both for radiotherapy, essentially extending the margins of the treatment volume, and for low-dose radiation protection, essentially increasing the number of cells affected by a low radiation dose.

In the radiotherapy context, even a bystander signal range as large as 1 mm would suggest that the bystander effect is unlikely to be a confounding factor at the margins of a radiotherapy treatment volume in the context of the larger uncertainties due to setup variations and organ motion (41).

By contrast, in the context of low-dose radiation risk assessment, an effective bystander signal range of ≈1 mm would imply that far more cells could be affected by a very low dose of radiation than expected based on simple target theory. Thus, bystander responses may potentially play a significant role in the extrapolation of radiation risks in humans from high doses to very low doses where nonhit bystander cells will predominate; simple extrapolations based on the number of cells directly hit may well be inadequate (42). At this point, it is not known whether a single α-particle can initiate the types of effects observed here in three-dimensional tissue: In single-cell studies, single α-particles have been reported to induce bystander effects for some endpoints (43) but not for others (6).

This work was supported by U.S. Department of Energy Low Dose Radiation Program Grants DE-FG02-03ER63632 and DE-FG02-01ER63226 and National Institutes of Health Grants P41 EB002033-09 and P01 CA-49062.

1. Nagasawa, H. & Little, J. B. (1992) *Cancer Res.* **52,** 6394–6396.
2. Morgan, W. F. (2003) *Radiat. Res.* **159,** 567–580.
3. Zhou, H., Randers-Pehrson, G., Waldren, C. A., Vannais, D., Hall, E. J. & Hei, T. K. (2000) *Proc. Natl. Acad. Sci. USA* **97,** 2099–2104.
4. Lorimore, S. A. & Wright, E. G. (2003) *Int. J. Radiat. Biol.* **79,** 15–25.
5. Ostreicher, J., Prise, K. M., Michael, B. D., Vogt, J., Butz, T. & Tanner, J. M. (2003) *Strahlenther. Onkol.* **179,** 69–77.
6. Sawant, S. G., Randers-Pehrson, G., Geard, C. R., Brenner, D. J. & Hall, E. J. (2001) *Radiat. Res.* **155,** 397–401.
7. Goldberg, Z. & Lehnert, B. E. (2002) *Int. J. Oncol.* **21,** 337–349.
8. Mothersill, C. & Seymour, C. (2001) *Radiat. Res.* **155,** 759–767.
9. Azzam, E. I., de Toledo, S. M. & Little, J. B. (2001) *Proc. Natl. Acad. Sci. USA* **98,** 473–478.
10. Suzuki, M., Zhou, H., Geard, C. R. & Hei, T. K. (2004) *Radiat. Res.* **162,** 264–269.
11. Nagar, S., Smith, L. E. & Morgan, W. F. (2003) *Cancer Res.* **63,** 324–328.
12. Brenner, D. J. & Sachs, R. K. (2002) *Int. J. Radiat. Biol.* **78,** 593–604.
13. Belyakov, O. V., Folkard, M., Mothersill, C., Prise, K. M. & Michael, B. D. (2002) *Radiat. Prot. Dosimetry* **99,** 249–251.
14. Belyakov, O. V., Folkard, M., Mothersill, C., Prise, K. M. & Michael, B. D. (2003) *Br. J. Cancer* **88,** 767–774.
15. Mothersill, C., O'Malley, K. & Seymour, C. B. (2002) *Radiat. Prot. Dosimetry* **99,** 163–167.
16. Barcellos-Hoff, M. H. & Brooks, A. L. (2001) *Radiat. Res.* **156,** 618–627.
17. Randers-Pehrson, G., Geard, C. R., Johnson, G., Elliston, C. D. & Brenner, D. J. (2001) *Radiat. Res.* **156,** 210–214.
18. Sawant, S. G., Zheng, W., Hopkins, K. M., Randers-Pehrson, G., Lieberman, H. B. & Hall, E. J. (2002) *Radiat. Res.* **157,** 361–364.
19. Schettino, G., Folkard, M., Michael, B. D. & Prise, K. M. (2005) *Radiat. Res.* **163,** 332–336.
20. Cannon, C. L., Neal, P. J., Southee, J. A., Kubilus, J. & Klausner, M. (1994) *Toxicol. in Vitro* **8,** 889–891.
21. Netzlaff, F., Lehr, C. M., Wertz, P. W. & Schaefer, U. F. (2005) *Eur. J. Pharm. Biopharm.* **60,** 167–178.
22. Monteiro-Riviere, N. A., Inman, A. O., Snider, T. H., Blank, J. A. & Hobson, D. W. (1997) *Microsc. Res. Tech.* **37,** 172–179.
23. Ponec, M., Boelsma, E., Gibbs, S. & Mommaas, M. (2002) *Skin Pharmacol. Appl. Skin Physiol.* **15,** Suppl. 1, 4–17.
24. Zhao, J. F., Zhang, Y. J., Kubilus, J., Jin, X. H., Santella, R. M., Athar, M., Wang, Z. Y. & Bickers, D. R. (1999) *Biochem. Biophys. Res. Commun.* **254,** 49–53.
25. Faller, C. & Bracher, M. (2002) *Skin Pharmacol. Appl. Skin Physiol.* **15,** Suppl. 1, 74–91.
26. Dymnikov, A. D., Brenner, D. J., Johnson, G. & Randers-Pehrson, G. (2000) *Rev. Sci. Instrum.* **71,** 1646–1650.
27. Boonstra, H., Oosterhuis, J. W., Oosterhuis, A. M. & Fleuren, G. J. (1983) *Virchows Arch. A Pathol. Anat. Histopathol.* **402,** 195–201.
28. Allen, R. T., Hunter, W. J., III, & Agrawal, D. K. (1997) *J. Pharmacol. Toxicol. Methods* **37,** 215–228.
29. Ponnaiya, B., Jenkins-Baker, G., Brenner, D. J., Hall, E. J., Randers-Pehrson, G. & Geard, C. R. (2004) *Radiat. Res.* **162,** 426–432.
30. Santner, T. J. & Duffy, D. L. (1989) *The Statistical Analysis of Discrete Data* (Springer, New York).
31. Agresti, A. (1990) *Categorical Data Analysis* (Wiley, New York).
32. Prise, K. M., Belyakov, O. V., Folkard, M. & Michael, B. D. (1998) *Int. J. Radiat. Biol.* **74,** 793–798.
33. Brenner, D. J., Little, J. B. & Sachs, R. K. (2001) *Radiat. Res.* **155,** 402–408.
34. Batsilas, L., Berezhkovskii, A. M. & Shvartsman, S. Y. (2003) *Biophys. J.* **85,** 3659–3665.
35. Dent, P., Yacoub, A., Contessa, J., Caron, R., Amorino, G., Valerie, K., Hagan, M. P., Grant, S. & Schmidt-Ullrich, R. (2003) *Radiat. Res.* **159,** 283–300.
36. Pribyl, M., Muratov, C. B. & Shvartsman, S. Y. (2003) *Biophys. J.* **84,** 883–896.
37. Shvartsman, S. Y., Hagan, M. P., Yacoub, A., Dent, P., Wiley, H. S. & Lauffenburger, D. A. (2002) *Am. J. Physiol.* **282,** C545–C559.
38. Monk, N. A. (1998) *Bull. Math. Biol.* **60,** 901–918.
39. Reilly, K. M. & Melton, D. A. (1996) *Cell* **86,** 743–754.
40. Gerashchenko, B. I. & Howell, R. W. (2003) *Cytometry A* **56,** 71–80.
41. Fenwick, J. D. & Nahum, A. E. (2001) *Med. Phys.* **28,** 560–569.
42. Brenner, D. J. & Sachs, R. K. (2003) *Health Phys.* **85,** 103–108.
43. Belyakov, O. V., Malcolmson, A. M., Folkard, M., Prise, K. M. & Michael, B. D. (2001) *Br. J. Cancer* **84,** 674–679.